45. Industrial ecology and integrated assessment: an integrated modeling approach for climate change

Michel G.J. den Elzen and Michiel Schaeffer

This chapter describes the background and modeling approaches used in simple climate models (SCMs) (Harvey *et al.* 1997). In general, SCMs are the simplified models used by the Intergovernmental Panel on Climate Change (IPCC) to provide projections of the atmospheric concentrations of greenhouse gases, global mean temperature and sea-level change response using as input emissions scenarios describing the future developments in the emissions of greenhouse gases. SCMs are computationally more efficient than more complex, computationally expensive three-dimensional models such as atmosphere–ocean general circulation models (AOGCMs). SCMs are therefore particularly suitable for multiple scenario studies, uncertainty assessments and analysis of feedbacks. The SCM approach is illustrated by applying one such model, meta-IMAGE (den Elzen 1998), to uncertainty analysis.

The SCM meta-IMAGE is a simplified version of the more complex climate assessment model IMAGE 2. IMAGE 2 aims at a more thorough description of the complex, long-term dynamics of the biosphere–climate system at a geographically explicit level ($0.5° \times 0.5°$ latitude–longitude grid) (Alcamo *et al.* 1996, 1998). Meta-IMAGE is a more flexible, transparent and interactive simulation tool that adequately reproduces the IMAGE-2.1 projections of global atmospheric concentrations of greenhouse gases, temperature increase and sea-level rise for the various IMAGE 2.1 emissions scenarios (see Figure 45.1). Meta-IMAGE consists of an integration of a global carbon cycle model (den Elzen *et al.* 1997), an atmospheric chemistry model and a climate model (upwelling-diffusion energy balance box model of Wigley and Schlesinger 1985 and Wigley and Raper 1992). The climate model also includes global temperature impulse response functions (IRFs; see, for example, Hasselmann *et al.* 1993) based on simulation experiments with various AOGCMs (den Elzen and Schaeffer 2001). This core model has lately been supplemented by a climate 'attribution' module, which calculates the regional contributions to various categories of emissions, concentrations of greenhouse gases and temperature and sea-level rise, especially developed for the evaluation of the Brazilian Proposal (UNFCCC 1997). Meta-IMAGE itself forms an integral part of the overall FAIR model (Framework to Assess International Regimes for burden sharing), which was developed to explore options for international burden sharing (den Elzen *et al.* 1999).

In the following section we describe a step-by-step approach along the cause and effect chain of climate change: from emissions to concentrations, from concentrations to radiative forcing and, finally, from radiative forcing to global mean surface-air temperature
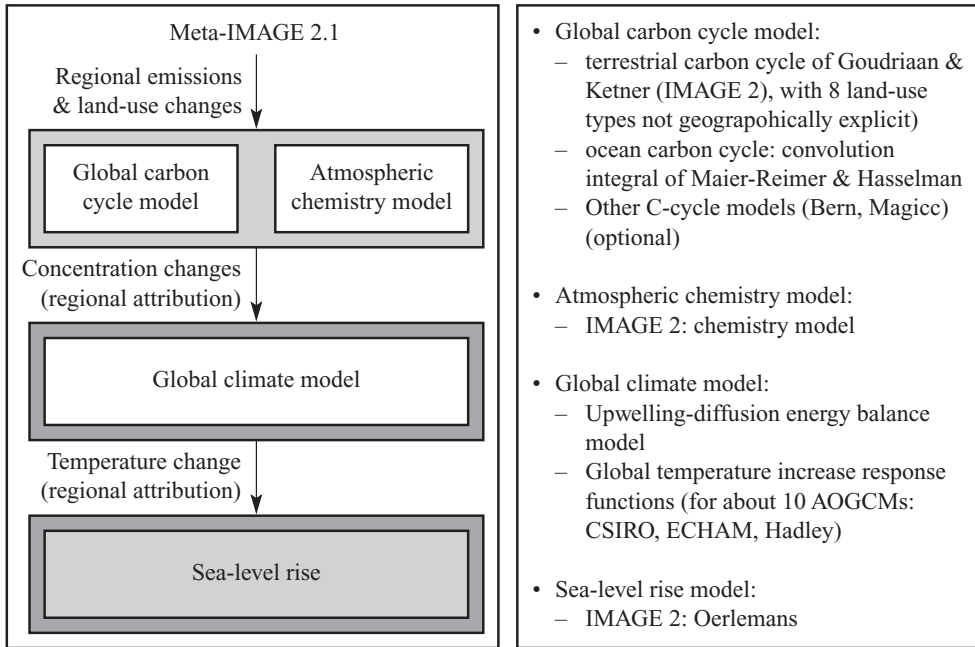
Figure 45.1   The climate assessment model meta-IMAGE 2.1 as used for the model analysis

increase. Various modeling approaches being used in SCMs, and in particular meta-IMAGE, are discussed. In the subsequent uncertainty analysis, we present an example of such a model analysis with meta-IMAGE of the impact of various carbon balancing mechanisms on the future projections of the atmospheric CO_2 concentration and the global mean temperature increase.

INTEGRATED MODELING APPROACH FOR CLIMATE CHANGE

From Emissions to Concentration

The concentration of a non-carbon dioxide greenhouse gas is modeled using a mass balance equation, in which the removal process in the stratosphere is proportional to the atmospheric concentration and inversely proportional to the atmospheric lifetime of a greenhouse gas. The same methodology is adopted in most current IPCC SCMs (Harvey *et al*. 1997). For nitrous dioxide (N_2O) and the halocarbons (including CFCs), a constant lifetime is used.

For methane (CH_4), matters are more complicated. Its chemical removal rate, and therefore its atmospheric lifetime, depend on the concentration of CH_4 itself. The latter is affected by the concentrations of other gases like NO_x, CO and VOCs. Therefore the lifetime of CH_4 is non-linearly dependent on the atmospheric composition. The lifetime of

CH_4 is time- and scenario-dependent and either the atmospheric chemistry has to be taken into account or the lifetime must be made time-dependent using previous results from (three-dimensional) chemical models. The current atmospheric lifetime is about nine years (Harvey *et al.* 1997). In addition to removal by chemical reactions in the atmosphere, CH_4 is also absorbed by soils, with a specific time constant of 150 years.

Regarding carbon dioxide (CO_2), there are considerable uncertainties in our knowledge of the present sources of and sinks for, the anthropogenically produced CO_2. In fact, the only well understood source is fossil fuel combustion while, in contrast, the source associated with land use changes is less understood. The amount of carbon remaining in the atmosphere is the only well known component of the budget. With respect to the oceanic and terrestrial sinks, the errors are likely to be in the order of ± 25 per cent and ± 100 per cent, respectively, mainly resulting from the lack of adequate data and from the deficient knowledge of the key physiological processes within the global carbon cycle (for example, Schimel *et al.* 1995). The uncertainties can be expressed explicitly in a basic mass conservation equation reflecting the global carbon balance (all components in gigatons of carbon content per year = GtC/yr):

$$\frac{dC_{CO2}}{dt} = E_{fos} + E_{land} - (S_{oc} + E_{for} + I), \tag{45.1}$$

where dC_{CO2}/dt is the change in atmospheric CO_2, E_{fos} is the CO_2 emission from fossil fuel burning and cement production, E_{land} the CO_2 emission from land-use changes, S_{oc} the CO_2 uptake by the oceans and E_{for} the CO_2 uptake through forest regrowth. To balance the carbon budget, a remaining term, I, which represents the missing sources and sinks, is introduced. I might therefore be considered as an apparent net imbalance between the sources and sinks. Analysis of the net imbalance in the global carbon cycle has become a major issue since the first IPCC scientific assessment report (IPCC 1990). Table 45.1 presents the global carbon balance over 1980–89 in terms of anthropogenically induced perturbations to the natural carbon cycle, as given by the IPCC (Schimel *et al.* 1995). Schimel *et al.* stated that the remaining imbalance of 1.3 ± 1.5 GtC/yr might be attributable to terrestrial sink mechanisms, those are the terrestrial feedbacks of CO_2 and N fertilization and the temperature feedbacks on net primary production and soil respiration.

Table 45.1   Components of the carbon dioxide mass balance, 1980–89, in terms of anthropogenically induced perturbations to the natural carbon cycle

Component GtC/yr	1980–89
Emissions from fossil fuel burning and cement production (E_{fos})	5.5 ± 0.5
Net emissions from land use change (E_{land})	1.6 ± 1.0
Change in atmospheric mass of CO_2 (dC_{CO2}/dt)	3.3 ± 0.2
Uptake by the oceans (S_{oc})	2.0 ± 0.8
Uptake by northern hemisphere forest regrowth (E_{for})	0.5 ± 0.5
Net imbalance [$I = (E_{fos} + E_{land}) - (dC_{CO2}/dt + S_{oc} + E_{for})$]	1.3 ± 1.6

Source: Schimel *et al.* (1995).

The concentration of CO_2 is calculated in carbon cycle models on the basis of the mass balance as described in equation (45.1). The models consist of a well mixed atmosphere linked to oceanic and terrestrial biospheric compartments. The oceanic component can be formulated as an upwelling-diffusion model (Siegenthaler and Joos 1992) or can be represented by a mathematical function (known as a convolution integral), which can be used to closely replicate the behavior of other oceanic models (Harvey 1989; Wigley 1991) such as in MAGICC (Wigley and Roper, 1992) and meta-IMAGE. The terrestrial component in both models is vertically differentiated into carbon reservoirs such as vegetation biomass, detritus, topsoil, deep soil and stable humus (Harvey 1989). For meta-IMAGE only, this component is also horizontally differentiated into eight land-use types: forests, grasslands, agriculture and other land for the developing and industrialized world (den Elzen 1998), which allows us to analyze the effect of land-use changes such as deforestation on the global carbon cycle.

To obtain a balanced past carbon budget in these models and therefore a good fit between the historical observed and simulated atmospheric CO_2 concentration, it is essential to introduce additional terrestrial sinks. Meta-IMAGE uses the CO_2 fertilization feedback and the temperature feedback on net primary production and soil respiration. Although the *N* fertilization feedback was included in the earlier version of the meta-IMAGE model (den Elzen *et al.* 1997), this feedback is, because of the consistency requirement with the IMAGE model, now excluded (den Elzen 1998). The parameterizations of these feedbacks have been derived from experiments with the IMAGE 2.1 model.

From Concentration to Radiative Forcing

Increased concentrations of greenhouse gases in the atmosphere lead to a change in the radiation balance. The basic effect is that the atmosphere becomes less transparent to thermal radiation. More heat is retained, although a number of climate feedbacks complicate this picture (Schimel *et al.* 1995). A good indicator for the change in radiation balance is radiative forcing. Radiative forcing is defined as the deviation from the pre-industrial radiative balance at the tropopause (border between troposphere and stratosphere) as a result of changes in greenhouse gas concentrations (while allowing the stratosphere to adjust to thermal equilibrium). This radiative forcing drives the changes in the free atmosphere and is the principal determinant for a change in surface air temperature. This results from the fact that the surface, planetary boundary layer and troposphere are so tightly coupled that they have to be treated as one thermodynamic system. The change in radiative balance at the tropopause then determines the change in energy input and outflow of that system.

Well mixed gases (gases with a lifetime longer then the mixing time of the atmosphere) have a uniform concentration throughout the atmosphere. When using a global average for the vertical profile of temperature, water vapor and clouds, an assessment can be made of the global average radiative forcing response to an increase in the concentration of a particular greenhouse gas.

Each gas absorbs radiation in certain frequency intervals called 'absorption bands'. If the concentration of a greenhouse gas is low, the troposphere will generally be transparent to radiation at the frequency of absorption of that gas. An increase of concentration leads to a practically linear increase in radiative forcing. This applies to the halocarbons, for example. As the concentration of a greenhouse gas increases, this dependence of

forcing on concentration gradually 'saturates', as in the case of CO_2, CH_4 and N_2O. For these gases, the net flux at the tropopause at the frequency of strongest absorption is already close to zero. The change in net flux resulting from increased concentration will therefore also be small. Increased concentration will, however, still lead to increased absorption at the edges of the strongest absorption bands and at weaker bands. The saturation effect is strongest for CO_2 and somewhat less so for CH_4 and N_2O.

Another complication is that some greenhouse gases absorb radiation in each other's frequency domains. This is called 'the overlap effect' and is especially relevant for methane and nitrous oxide. Increases in CH_4 concentration decrease the efficiency of N_2O absorption and vice versa. The present SCMs like meta-IMAGE use the global radiative forcing dependencies of the IPCC (Harvey *et al.* 1997), including the major saturation and overlap effects.

From Radiative Forcing to Global Mean Temperature Increase

The large heat capacity of the oceans plays an important role in the time-dependent response of the climate system to external forcing, such as increased concentrations of greenhouse gases. Because the heat capacity of land surface and atmosphere is very small, ignoring inner ocean response would mean that, after a disturbance, the climate system would settle into a new equilibrium within a few years. However, heat is transported from the rapidly adjusting mixed (upper) layer of the ocean to deeper layers. This heat is therefore not available to warm the surface layer. Sea surface temperatures will rise more slowly. As a result, surface air temperatures over the ocean *and* land also increase more slowly. The time needed for the coupled atmosphere–ocean system to adjust fully to disturbances is extended.

Hasselmann *et al.* (1993) have shown that the time-dependent temperature response of coupled AOGCMs can be very well described using a linear combination of exponential decay terms, called impulse response functions (IRFs). As explained in Hasselmann *et al.* (1993), IRFs form a simple tool to describe ('mimic') mathematically transient climate model response to external forcing. A two term IRF model as used here (as in Hasselmann *et al.* 1993) is based on the following convolution integral, relating global mean temperature response ΔT to time-dependent external forcing $Q(t)$:

$$\Delta T(t) = \frac{\Delta T_{2\times}}{Q_{2\times}} \int_{t_0}^{t} Q(t') \left(\sum_{s=1}^{2} l_s \frac{1}{\tau_s} e^{\frac{t-t'}{\tau_s}} \right) dt', \qquad (45.2)$$

where $Q_{2\times}$ is the radiative forcing for a doubling of CO_2 and $\Delta T_{2\times}$ is the climate sensitivity, that is, the long-term (equilibrium) annual and global mean surface air temperature increase for a doubling of CO_2 concentration. The climate sensitivity is an outcome of all geophysical feedback mechanisms and their associated uncertainties, and is lying within the range of 1.5 to 4.5°C, with a 'best guess' value of 2.5°C; l_s is the amplitude of the 1st or 2nd component with exponential adjustment time constant τ_s, while $l_1 + l_2 = 1$. One of the two terms of these IRFs describes the rapid response and the other the slower response. The rapid response part dominates the response on a time scale of a few decades. This means effectively that the slower response part is of little relevance if the policy horizon only extends over a few decades. Still, a significant part (roughly 50 per cent) of the final global warming will manifest itself decades to centuries later. Called the 'warming commitment', this is also what causes sea-level rise to continue long after stabilization of greenhouse gas concentrations. The heat transport processes discussed above

determine the balance between the fast and slow adjustment terms. This balance is still a source of uncertainty. Mathematically, the two term IRF approach is equivalent to a two box energy balance model. However, these boxes respond independently to the forcing. This makes it impossible to readily link the different IRF terms to specific elements in the physical climate system, such as mixed layer and deeper ocean.

Therefore the more physically based approach of the linked multi-box energy balance climate model is more often applied in SCMs. The original version of this type of model is described in Wigley and Schlesinger (1985) and Wigley and Raper (1992), although it has been modified since to include different climate sensitivities for land and oceans, and a variable ocean upwelling rate. The basic heat balance equation is described as follows:

$$C_m \frac{d\Delta T_o(t)}{dt} = Q(t) - \lambda \Delta T_o(t) - \Delta F(t), \tag{45.3}$$

where C_m is the heat capacity of the ocean mixed layer (Watts per year over degrees C times meters squared $= Wm^{-2}°C^{-1}$), $Q(t)$ the total radiative forcing (W/m²), ΔT_o the change in temperature of the ocean mixed layer (°C), ΔF the change in heat flux from the mixed layer to deeper ocean layers (W/m²) and l the climate sensitivity parameter ($Wm^{-2}°C^{-1}$), that is: $Q_{2\times}/\Delta T_{2\times}$, with: $Q_{2\times}$ being the radiative forcing for a doubled atmospheric CO_2 concentration ($= 4.37$ W/m²; Harvey *et al.* 1997). ΔF is calculated from the diffusion parameter and the transport terms.

As a reference climate model in meta-IMAGE, we use the upwelling-diffusion box climate model as described above, with a default climate sensitivity of $\Delta T_{2\times} = 2.35°C$ to match IMAGE 2.1 results. For alternative temperature calculations, we also use a set of IRFs, with parameter settings derived from a range of AOGCMs (den Elzen and Schaeffer 2001).

From Global Mean Temperature Increase to Sea Level Rise

Global warming is expected to cause a sea level rise due to ocean expansion, the melting of glaciers and ice caps, and the changes in the volume of the Greenland and Antarctic ice sheets. These processes are represented in the model by simple dynamic relationships presented by Oerlemans (1989) and Alcamo *et al.* (1998), using the parameterizations of den Elzen (1998).

MODEL EXPERIMENTS

The following uncertainty analysis presents an application of the integrated climate change cause-and-effect chain model described in the previous section. In this analysis several carbon cycle model parameters are adjusted to let the model's carbon cycle output 'browse' the uncertainty range of observed carbon budget components (Table 45.1). We then compare this uncertainty range with the uncertainty in climate system response. Finally, the synergy between these two major sources of uncertainty in climate change assessments is highlighted.

Input Data

The main input data of meta-IMAGE are composed of the anthropogenic emissions of the greenhouse gases and the land use changes. The fossil fuel CO_2 emissions for the period

1751–1995 are based on the CO_2 emissions database of the Oak Ridge National Laboratory (ORNL) – CO_2 Data and Information Assessment Center (CDIAC) (Marland and Rotty 1984; Marland *et al. 1*999; Andres *et al.* 1999). The ORNL–CDIAC emission data are limited to CO_2 emissions from fossil fuels and cement production. The historical anthropogenic emissions of the other non-CO_2 greenhouse gas emissions and SO_2 are therefore taken from the EDGAR (Emission Database for Global Atmospheric Research) data set (Olivier *et al.* 1996) and the HYDE database (Klein-Goldewijk and Battjes 1997). The 1995–2100 anthropogenic emissions of all greenhouse gases and SO_2 are based on the IMAGE 2.1 Baseline-A scenario (Alcamo *et al*. 1998). This forms a 'business as usual' scenario, one without implementation of explicit climate change mitigation policies. The historical CO_2 emissions from land-use changes are based on Houghton and Hackler (1995) and Houghton *et al.* (1987). The land-use changes, important for the terrestrial carbon cycling processes, are also based on Houghton and Hackler (1995), but further disaggregated in the four major land cover types: forests, grasslands, agriculture and other land, for the developing and industrialized world, as used in meta-IMAGE. The area changes for the above four land-use categories for the developing and industrialized world for the period 1990–2100 are also based on aggregated land-use data of the IMAGE 2.1 Baseline-A scenario. The same holds for the 1995–2100 regional CO_2 emissions from land-use changes.

Various Balancing Approaches for the Past Carbon Budget

A key principle in the model analysis here is that we define different assumptions for the terrestrial biogeochemical feedbacks in order to balance the past carbon budgets; and subsequently, future atmospheric CO_2 concentration projections are made. In the reference case, model parameters representing the key terrestrial feedbacks (that is, the CO_2 fertilization effect and temperature feedback on net primary production and soil respiration) and oceanic uptakes are set at the default values used within meta-IMAGE. This leads to a balanced past carbon budget and a good fit between the historically observed and simulated CO_2 concentrations. The simulated carbon fluxes of the components of the carbon budget for the 1980s (1980–89) are similar to the IPCC estimates (Table 45.2). In the sensitivity experiments the scaling factors for the ocean flux, emissions from land use changes, northern hemispheric terrestrial uptake and CO_2 fertilization feedback parameters are varied so that all parameter combinations will lead to a well balanced past carbon budget. The temperature feedback parameters are kept at their default values. The simulated carbon fluxes of the carbon budget, that is, the oceanic and terrestrial carbon uptake and the CO_2 emissions from land use changes during the 1980s should be between the upper and lower boundaries of the IPCC estimates (Table 45.2). In the first two extreme 'oceanic uptake' cases, a high and a low oceanic uptake, the scaling factor for the ocean flux is set at the maximum and minimum values. This leads to the 1980s oceanic uptake of 3.0 and 1.0GtC/yr, respectively. The balanced past carbon budget is now achieved by scaling the CO_2 fertilization feedback parameters and the northern hemispheric terrestrial uptake. The terrestrial sink for the 1980s then varies between 0.8 and 2.3GtC/yr (Table 45.2). These two cases have been selected from other similar conditioned simulation experiments as two extreme examples of the balancing variations in the terrestrial and oceanic uptake fluxes (representing the terrestrial and oceanic uncertainties, in which the impact of variations in the temperature feedback parameters is ignored). The resulting projected CO_2 concentra-

Table 45.2   *Components of the carbon budget (in GtC/yr), 1980–89, according to the IPCC (Schimel* et al. *1995) and model simulations for the carbon balancing experiments*

Component	IPCC estimate	Reference case	High oceanic uptake	Low oceanic uptake	High deforestation	Low deforestation
CO_2 emissions from fossil fuel burning and cement production (E_{fos})	5.5 ± 0.5	5.5	5.5	5.5	0.0	5.5
CO_2 emissions from land-use changes (E_{land})	1.6 ± 1.0	1.6	1.6	1.6	2.6	0.6
Change in atmospheric CO_2 (dC_{CO2}/dt)	3.3 ± 0.2	3.3	3.3	3.3	3.3	3.3
Uptake by the oceans (S_{oc})	2.0 ± 0.8	2.0	3.0	1.0	2.0	2.0
Uptake by northern hemisphere forest regrowth (E_{for})	0.5 ± 0.5	0.5	0.0	0.5	0.5	0.5
Additional terrestrial sinks (IPCC: $[E_{fos} + E_{land}] - [dC/dt^* + E_{for} + S_{oc}]$)	1.3 ± 1.6	1.3	0.8	2.3	2.3	0.3

tion range in 2100 varies between 687 and 719ppmv, while the 2100 concentration is 717ppmv for the reference case (dark gray area in Figure 45.2(b)).

Further experiments consider the uncertainties in the CO_2 emissions from land-use changes (land-use sources and carbon sink uncertainties) by setting its scaling factor at maximum and minimum values (emissions during the 1980s between 0.6–2.6GtC/yr) (Table 45.2). The extreme upper and lower CO_2 concentration projections are now achieved (662 and 794 ppmv, respectively, by 2100), by balancing the past carbon budget with only the CO_2 fertilization effect, while the oceanic parameters are kept constant (light gray area in Figure 45.2(b)). Summarized, these experiments show that various balanced past carbon budgets in the model lead to a range in the 2100 atmospheric CO_2 concentration for the IMAGE Baseline A scenario of about 10 per cent above and below the central projection of ~717ppmv.

Figure 45.2 shows the temperature increase for the Baseline-A scenario using the CO_2 concentration pathway from the reference case according to the meta-IMAGE climate model (solid line). In Figure 45.2(a), uncertainty of carbon cycle modeling is illustrated, given by uncertainty in terrestrial and oceanic carbon sink fluxes (dark gray), and in the sink and land use sources (light gray). Figure 45.2(b) illustrates uncertainty in the climate system response as estimated by using different IRFs of AOGCMs. Dark gray: range of outcomes for IPCC's 'best guess' climate sensitivity of 2.5°C combined with the IRF time scale parameters of the AOGCMs. Grey: IRF time scale parameters combined with their respective climate sensitivities. Light gray: IRF time scale parameters arbitrarily combined with climate sensitivities in the full IPCC range of 1.5–4.5°C. The two uncertainty ranges represent the uncertainties in the terrestrial and oceanic carbon sink fluxes (dark gray), and in the sink and land use sources (light gray).
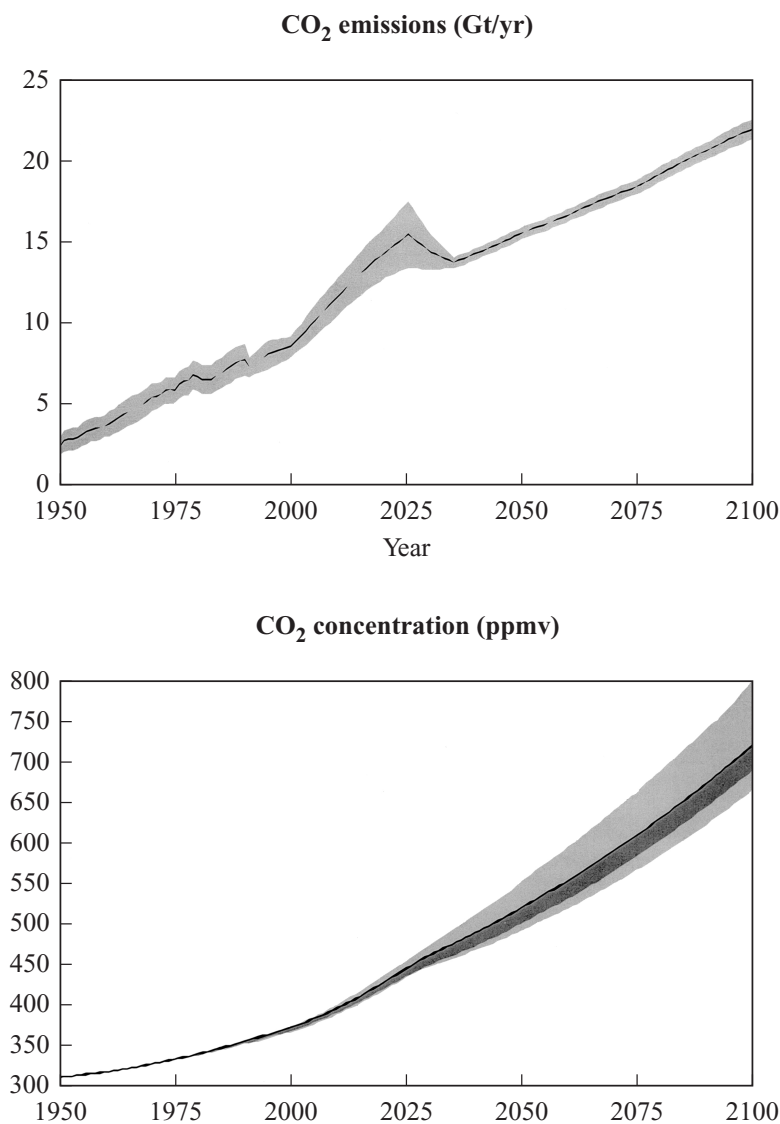
CO$_2$ emissions (Gt/yr)

CO$_2$ concentration (ppmv)

*Figure 45.2   Global anthropogenic CO$_2$ emissions (a) and CO$_2$ concentrations (b)
Baseline-A scenario according to the meta-IMAGE model for the carbon
balancing experiments*

Using Temperature Response Functions of Various AOGCMS

We now apply the results of a number of climate models to reflect uncertainty in climate modeling. In order to do so, we have diagnosed a range of different response time scale parameters and climate sensitivities from sophisticated atmosphere–ocean climate models in den Elzen and Schaeffer (2000). Using this range results in the spread in projected tem-
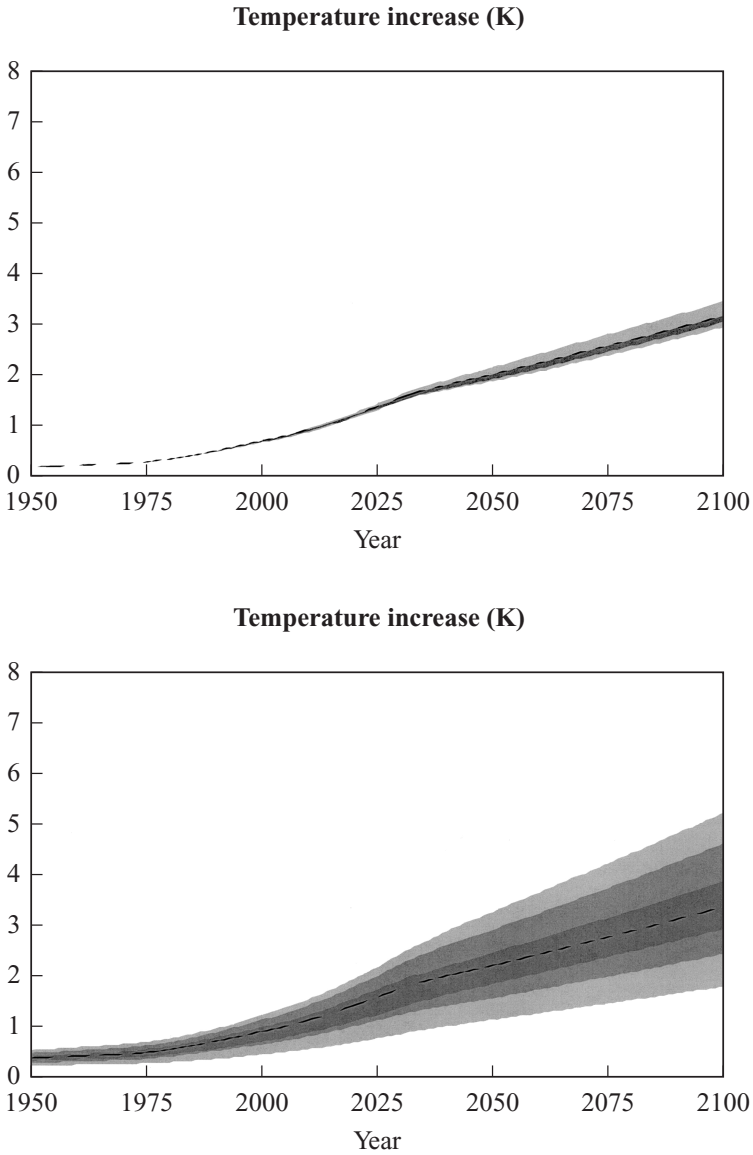
Temperature increase (K)

Temperature increase (K)

Figure 45.3   Global anthropogenic CO_2 emissions (a) and CO_2 concentration pathway (b) from the reference case according to the meta-IMAGE model

perature response shown in Figure 45.3 (gray area). Here the solid line represents the temperature response of our meta-IMAGE reference case, which is not necessarily the most likely. The global surface temperature increase for the reference projection is about 3.1°C for the period 1751 (pre-industrial) to 2100 for the reference case. The innermost, dark gray area depicts the range of results if all the different IRF time scale parameters are applied using the same IPCC 'best guess' climate sensitivity of 2.5°C. The uncertainty

Applications and Policy Implications

range broadens significantly if the IRF time scale parameters are combined with their respective climate sensitivities, ranging from 1.58 to 3.7°C. Finally, the range broadens even further if the IRF time scale parameters are arbitrarily combined with climate sensitivities from the full IPCC range of 1.5–4.5°C (light gray). Figure 45.3 clearly shows that the climate sensitivity plays a dominant role in determining the range of absolute temperature increase.

Figure 45.3(a) illustrates the uncertainty of carbon cycle modeling as shown by terrestrial and oceanic carbon sink fluxes (dark gray), and in the sink and land use sources (light gray). Figure 45.3(b) illustrates uncertainty in the climate system response as estimated using different IRFs of AOGCMs. Dark gray: range of outcomes for IPCC's 'best guess' climate sensitivity of 2.5°C combined with the IRF time scale parameters of the AOGCMs. Grey: IRF time scale parameters combined with their respective climate sensitivities. Light gray: IRF time scale parameters arbitrarily combined with climate sensitivities in the full IPCC range of 1.5–4.5°C.

Overall Uncertainties of Global Carbon Cycle and Climate Models

Having analyzed the effect of some major uncertainties in the carbon cycle and climate in the preceding sections, we now compare their relative importance for projected temperature increase. In Figure 45.4, the central dark gray area depicts total uncertainty in the carbon cycle balancing exercise (compare with Figure 45.3(a), while the gray area reflects total uncertainty from climate modeling (compare with Figure 45.3(b)). Finally, the light gray area shows the resulting total range in outcomes using the overall uncertainties in the carbon cycle and climate. The extension of uncertainty on the upper side is worth noting;
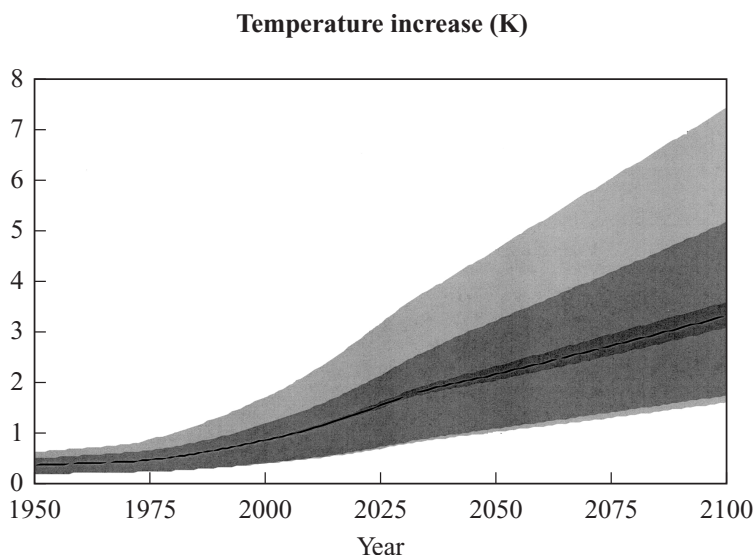
Temperature increase (K)

Figure 45.4   The global mean surface temperature increase for the Baseline-A scenario for the model uncertainties in the carbon cycle and climate models, and the combined effect of both

this is a result of the strong temperature feedback on soil respiration as it is triggered by a high temperature increase in meta-IMAGE when a high climate sensitivity is applied. Clearly, uncertainty in climate modeling is dominant in determining absolute temperature increase, caused by uncertainty in climate sensitivity. However, because of the temperature–respiration feedback, the 'synergy' of carbon cycle and climate system increases this uncertainty significantly. This forms a perfect illustration of the advantage of using an integrated modeling approach.

CONCLUSIONS

In this chapter we have described the cause-and-effect chain of climate change: from emissions and concentrations of greenhouse gases to global mean temperature and sea level rise. We briefly treated the modeling approaches being used in SCMs and in particular the integrated assessment model meta-IMAGE. Although the model representations of the biological, physical and chemical processes in these models are highly aggregated representations of complicated, geographically dependent and only partly know processes, SCMs prove to be valuable tools for describing the climate change problem in a quantitative, adequate way. SCMs are particularly useful in providing climate projections in multiple scenario studies and uncertainty assessments, as was shown in the illustrative model analysis.